

Small scale effects in the observable power spectrum at large angular scales

William L. Matthewson and Ruth Durrer

Université de Genève, Département de Physique Théorique and Centre for Astroparticle Physics,
24 quai Ernest-Ansermet, CH-1211 Genève 4, Switzerland

E-mail: william.matthewson@unige.ch, ruth.durrer@unige.ch

Abstract. In this paper we show how effects from small scales enter the angular-redshift power spectrum $C_\ell(z, z')$. In particular, we show that spectroscopic surveys with high redshift resolution are affected by small scales already on large angular scales, i.e. at low multipoles. Therefore, when considering the angular power spectrum with spectroscopic redshift resolution, it is important to account for non-linearities relevant on small scales even at low multipoles. This may also motivate the use of the correlation function instead of the angular power spectrum. These effects, which are very relevant for bin auto-correlations, but not so important for cross-correlations, are quantified in detail.

Contents

1	Introduction	1
2	Small scale contributions in low ℓ spectroscopic $C_\ell(z, z)$'s	2
3	Non-linearities in low ℓ spectroscopic $C_\ell(z, \sigma_z)$'s	4
4	Cross-correlations, $C_\ell(z_1, z_2)$ for $z_1 \neq z_2$	5
5	Conclusion	12

1 Introduction

In cosmology, positions of galaxies are truly observed as redshifts and angles. If we want to determine the correlation properties of galaxies (or classes of galaxies) in a model independent way, we must study the redshift-dependent angular power spectra, $C_\ell(z, z')$, or the angular correlation functions, $\xi(\theta, z, z')$. Assuming statistical isotropy, these 2-point functions fully determine the 2-point statistics of the galaxy distribution and, with the additional assumption of Gaussianity, they determine all statistical quantities. Whenever redshifts and angles are converted into length scales, assumptions about the background cosmology are made. At very low redshift, $z \ll 1$, the distance is entirely determined by the Hubble parameter, $r(z) \simeq z/H_0$ and the model dependence is encoded in the cosmological ‘unit of length’ given by $h^{-1}\text{Mpc}$, where $h = H_0/100\text{km/sec/Mpc}$. However, at redshifts of order unity and larger, the full cosmological model enters in the determination of $r(z)$. This fact has prompted a tendency in the field to prefer the directly-observable angular-redshift power spectra and correlation function. We cite Refs. [1–7] as examples.

In this paper we study the following question: When analyzing a spectroscopic dataset, in which redshifts are very well known, that is $\sigma_z \lesssim 10^{-3}$, does the precise radial information about the galaxy position affect the power spectrum at low multipoles of $\ell \lesssim 100$?

We shall see that the answer to this question is yes, as already noted in [8]. Here we perform a detailed study of the amplitude of the effect and its origin. We find that small scale non-linearities significantly affect spectroscopic $C_\ell(z, z)$'s, including at low ℓ . This finding is not so surprising and is actually at the origin of the fact that the Limber approximation totally fails for spectroscopic number count $C_\ell(z, z)$'s, see e.g. [9]. We study how these effects decay if we either smear out the $C_\ell(z, z)$'s over a sufficiently large redshift window or consider cross-correlations, $C_\ell(z, z')$ with sufficiently large $|z - z'|$. Contrary to correlations of galaxy number counts alone, lensing or lensing-number counts cross-correlations (galaxy-galaxy-lensing) are insensitive to small scale effects at low multipoles, due to the broad kernel of the shear and magnification integrals.

This paper is organized as follows: in the next section we study the imprint of small scale contributions on the $C_\ell(z, z)$'s from galaxy number counts. In Section 3 we quantify the effects of non-linearities at low ℓ 's and in Section 4 we investigate cross-correlations. We end with our conclusions.

2 Small scale contributions in low ℓ spectroscopic $C_\ell(z, z)$'s

If we consider correlations of galaxies at fixed redshift with small redshift uncertainty σ_z , their comoving radial separation is smaller than

$$r(z, \sigma_z) = \frac{\sigma_z}{H(z)}, \quad \text{corresponding to a radial wave number} \quad k_{\parallel}(z, \sigma_z) = \frac{2\pi H(z)}{\sigma_z}. \quad (2.1)$$

Typical spectroscopic surveys have redshift resolution of $\sigma_z \sim 10^{-3}$ or better. As an example, $r(1, 10^{-3}) = 1.7h^{-1}\text{Mpc}$, which is well within the non-linear regime at $z = 1$. To find a quantitative estimate, we consider the flat sky approximation for $C_\ell(z, z')$, which is excellent for very close redshifts [9].

$$C_\ell(z, z') = \frac{1}{2\pi r^2(\bar{z})} \int_{-\infty}^{\infty} dk_{\parallel} P_g(k, \bar{z}) e^{-ik_{\parallel}(z-z')/H(\bar{z})}, \quad (2.2)$$

where $\bar{z} = (z + z')/2$ is the mean redshift, $k = \sqrt{k_{\parallel}^2 + \ell^2/r^2(\bar{z})}$ and $P_g = b^2(z)P_m$ denotes the galaxy power spectrum. P_m is the matter power spectrum and $b(z)$ is the galaxy bias (we neglect non-linear bias). Integrating this over z and z' , with a tophat window of width σ_z centered at \bar{z} , we obtain

$$C_\ell(\bar{z}, \sigma_z) = \frac{1}{2\pi r^2(\bar{z})} \int_{-\infty}^{\infty} dk_{\parallel} P_g(k, \bar{z}) j_0^2\left(\frac{k_{\parallel}\sigma_z}{2H(\bar{z})}\right). \quad (2.3)$$

Strictly speaking, the above expression is for the density term only. In order to include redshift space distortions (RSD), we have to replace the power spectrum by

$$P_{D+RSD}(\mu, k, \bar{z}) = (b(z) + f(z)\mu^2)^2 P_m(k, \bar{z}),$$

where $\mu = k_{\parallel}/k$ is the direction cosine of \mathbf{k} with the forward direction and $f(z)$ is the growth rate, see e.g. [10]. This is the power spectrum which we use to determine the so-called ‘standard terms’ which comprise density and RSD correlations and which are used in the present analysis.

We have compared approximation (2.3) (replacing P_g by P_{D+RSD}) with the CLASS-code [11] and found that the difference is smaller than 1% for windows of size $\sigma_z < 0.01$. For larger windows the error slowly grows and reaches about 4% for $\sigma_z = 0.1$ and $\ell = 100$.

The spherical Bessel function, j_0 , acts as a ‘low-pass filter’, meaning that only modes with $k_{\parallel} \leq 2\pi H(\bar{z})/\sigma_z =: k_{\parallel}(z, \sigma_z)$ significantly contribute to the angular power spectrum. The smaller σ_z , the higher the values of k_{\parallel} which contribute. In Fig. 1 we plot $k_{\parallel}(z, \sigma_z)$ as a function of redshift for some values of σ_z .

Clearly, only for values of ℓ with $k_{\parallel}(z, \sigma_z) \lesssim \ell/r(z)$ can the Limber approximation, which replaces $k = \sqrt{k_{\parallel}^2 + \ell^2/r^2(z)}$ by $(\ell + 1/2)/r(z)$, be a reasonable approximation. Inserting $k_{\parallel}(z, \sigma_z)$, we find that this requires $\ell > \ell(z, \sigma_z)$, with

$$\ell(z, \sigma_z) = 2\pi H(\bar{z})r(z)/\sigma_z = 2\pi \int_0^z dz' \frac{H(z)}{H(z')} > 2\pi \frac{z}{\sigma_z}. \quad (2.4)$$

For $z \sim 1$ and $\sigma_z \lesssim 10^{-3}$, $\ell(z, \sigma_z) > 6000$, and we shall see that non-linearities enter the entire spectrum $C_\ell(z)$.

Of course, the extent to which the contributions from high k_{\parallel} are relevant also depends on the shape of the power spectrum. For example, we expect them to be more relevant for the non-linear power spectrum which is boosted, especially at small scales.

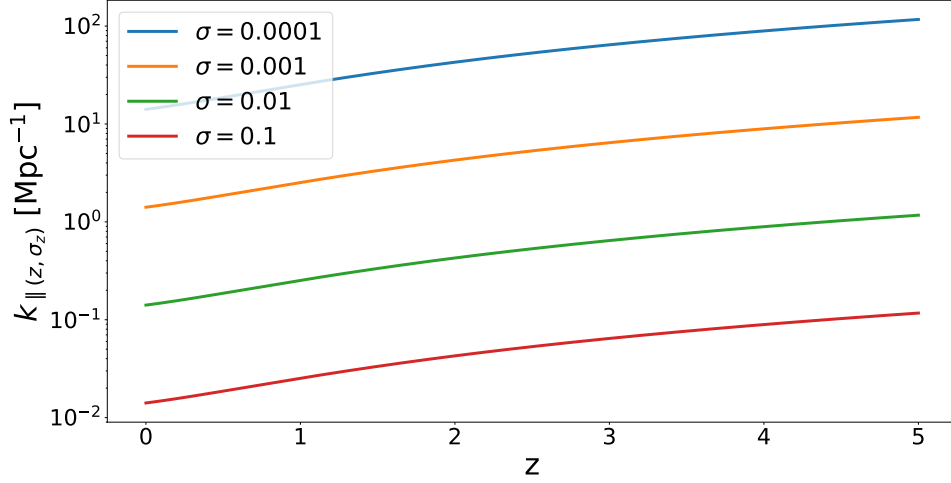


Figure 1. We show $k_{\parallel}(z, \sigma_z)$ as a function of redshift, with different colours indicating different values of σ_z ranging from 10^{-4} to 10^{-1} . As is clear from the second part of (2.1), for wider redshift windows the most important contributions to the spectrum come from smaller value of k_{\parallel} .

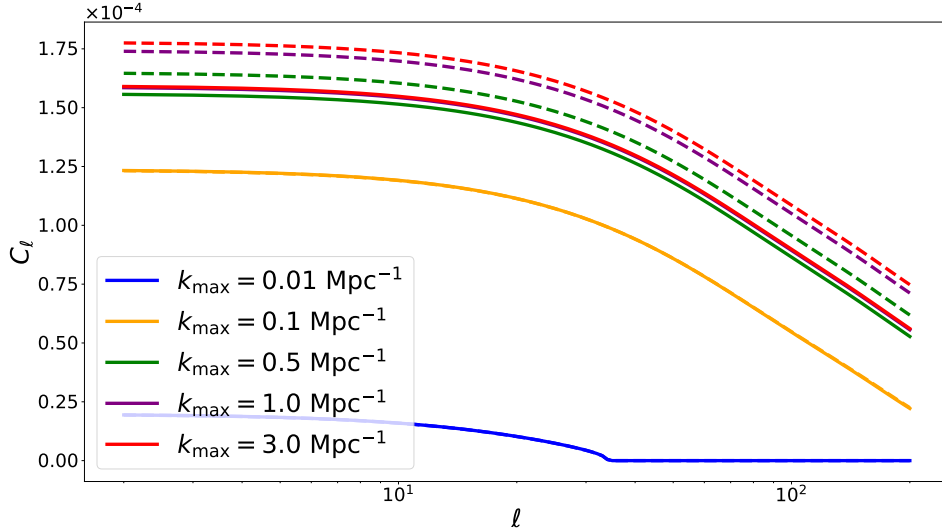


Figure 2. We show $C_{\ell}(\bar{z} = 1, \sigma_z = 10^{-3})$ computed using various values of k_{\max} , shown in different colours. The solid lines represent the linear spectra, while the dashed lines represent the halofit corrections. As k_{\max} increases, the spectra converge to their accurate values at each ℓ . For the lowest values of k_{\max} , the spectrum at higher ℓ 's does not obtain any contributions from the range of k considered, and drops to zero. The difference between the linear spectrum and halofit increases with k_{\max} . The spectra for $k_{\max} = 1/\text{Mpc}$ and $k_{\max} = 3/\text{Mpc}$ are very close, which indicates that the spectrum is converging at $k_{\max} \simeq 3/\text{Mpc}$.

Our numerical results at unequal redshift are obtained with the code ‘CAMB sources’ [2] which allows for a simpler adjustment of the k_{\max} in the integration of the spectra than CLASS.

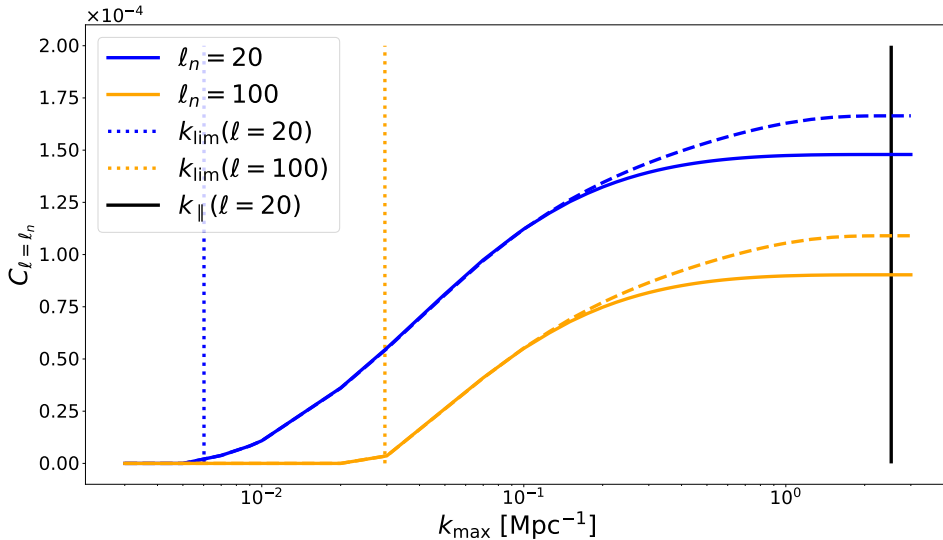


Figure 3. We show $C_{20}(\bar{z} = 1, \sigma_z = 10^{-3})$ (blue) and $C_{100}(\bar{z} = 1, \sigma_z = 10^{-3})$ (orange) from the linear (solid lines) and halo-fit (dashed lines) power spectra as a functions of k_{\max} , the upper boundary of the k -integral. The values of $k_{\parallel}(z, \sigma_z)$ and $k_{\text{Lim}}(\ell, z)$ are also indicated. From this plot we see that $k_{\max} \simeq k_{\parallel}(z, \sigma_z)$ is required for the halo-fit spectra to converge.

For better stability in the case of unequal redshifts, we use Gaussian windows with full width at half maximum given by σ_z throughout. As an example, in Fig. 2 we plot $C_{\ell}(\bar{z} = 1, \sigma_z = 10^{-3})$, integrating up to different values of k_{\max} . The power missing for small k_{\max} at low ℓ is as significant as at high ℓ . Hence the value of ℓ is not simply related to the value of k which gives the dominant contribution to the angular power spectrum. For the lowest k_{\max} there is no difference between the linear power spectrum and halo-fit, but for $k_{\max} \gtrsim 0.1$ the halo-fit power spectrum boosts all C_{ℓ} 's. This shows that non-linearities also enter at low ℓ 's.

In Fig. 3 we plot C_{20} (blue) and C_{100} (orange) for $\bar{z} = 1, \sigma_z = 10^{-3}$ as functions of k_{\max} . As vertical lines we also indicate $k_{\parallel}(z, \sigma_z)$ (black) and $k_{\text{Lim}}(z, \ell) = (\ell + 1/2)/r(z)$ (dotted, blue and orange respectively). The value k_{\parallel} is roughly where convergence of the spectra is reached¹. It is evident that non-linearities have a significant effect, indicated by the dashed lines.

At $z = 1$ we obtain $k_{\text{Lim}} \simeq 4.36 \times 10^{-4}(\ell + 1/2)h/\text{Mpc}$ and $k_{\parallel}(z, \sigma_z = 10^{-3}) \simeq 3.75h/\text{Mpc}$. We use ΛCDM with $\Omega_m = 0.31$, $\Omega_{\Lambda} = 0.69$ and $h = 0.6732$ and $b(z) = 1$ for our numerical examples. The results are quite insensitive to the bias.

3 Non-linearities in low ℓ spectroscopic $C_{\ell}(z, \sigma_z)$'s

In the previous section we have seen that, even at low ℓ , spectroscopic $C_{\ell}(z, \sigma_z)$'s are affected by the power spectrum at high k 's. This implies that they are significantly affected by non-linearities even if $k_{\text{Lim}} \ll k_{\text{NL}}$. Let us introduce the non-linearity scale, as it is often defined, by [12, 13]

$$\sigma(R_{\text{NL}}, z) = 0.2. \quad (3.1)$$

¹Even though k_{\max} is the value of k not k_{\parallel} , this difference is irrelevant for $k_{\parallel} \gg k_{\text{Lim}}$, since in this regime $k \simeq k_{\parallel}(1 + \frac{1}{2}(k_{\text{Lim}}/k_{\parallel})^2)$.

Here $\sigma^2(R, z)$ is the usual variance of the mass fluctuation in a sphere of radius R ,

$$\sigma^2(R, z) \equiv \frac{1}{2\pi^2} \int_0^\infty \frac{dk}{k} \left(\frac{3j_1(kR)}{kR} \right)^2 k^3 P_m(k, z) \quad (3.2)$$

where P_m is the matter power spectrum. The amplitude of the matter power spectrum is actually often parametrized by $\sigma(R = 8\text{Mpc}/h, z = 0) = \sigma_8$. We associate it with the corresponding non-linearity wave-number,

$$k_{\text{NL}}(z) = \frac{2\pi}{R_{\text{NL}}(z)}. \quad (3.3)$$

In Fig. 4 we plot the k_{max} required to reach a precision of 1% (upper panel) and 5% (lower panel) for C_{20} (blue) and C_{100} (orange) as a function of σ_z . The non-linearity scale is also indicated (red line). At $\sigma_z = 10^{-3}$, $k_{\text{max}} \simeq 10k_{\text{NL}}$ for the halofit spectra, even at $\ell = 20$, for 1% accuracy and somewhat smaller for 5%. Up to $\sigma_z \simeq 10^{-2}$, spectra are affected by more than 5% by non-linear scales. The naive estimate of $k_{\text{max}} \sim k_{\parallel}(z, \sigma_z)$ overestimates the numerically calculated k_{max} , especially for smaller windows σ_z , where the figure shows that the contributions from k 's saturate and higher k contributions are not necessary to reach the level of precision considered.

In Fig. 5 we show the 1% accuracy values (upper panel) and 5% accuracy values (lower panel) of k_{max} for $\ell = 20$ (blue) and $\ell = 100$ (orange) for the halofit (dashed) and linear (solid) power spectra at fixed $\sigma_z = 10^{-3}$, typical of a spectroscopic survey, as functions of redshift. We also indicate $k_{\text{NL}}(z)$ (red). The required $k_{\text{max}}(z)$ is larger than $k_{\text{NL}}(z)$ throughout. Non-linearities still affect the spectra up to $z = 5$ by more than 5%. Note also that k_{max} depends only weakly on redshift for the linear power spectrum. Our naive estimates $k_{\text{max}} \sim k_{\parallel}(z, \sigma_z) = 2\pi H(z)/\sigma_z \simeq 2.5(H(z)/H(1))/\text{Mpc}$ (which again overestimates the convergence scale in all cases) would be rising with redshift. The near constancy of k_{max} is caused by the fact that the matter power spectrum decreases for $k > k_{\text{eq}} \sim 0.01/\text{Mpc}$. The rise in $k_{\parallel}(z, \sigma_z)$ and the decrease in the matter power spectrum seem to nearly balance each other in the linear power spectrum. However, the redshift dependence of k_{max} becomes quite pronounced for the non-linear (halofit) spectrum. It is therefore purely a consequence of the shape of the power spectrum, which decreases much less steeply when considering the non-linear case. The value of $k_{\text{max}}(z)$ for the halofit power spectrum first rises until about $z = 2$, a result of the competing effects of weakening non-linearities and the decreasing scale of modes probed by a fixed window width, and then decreases towards higher redshifts, slowly approaching the value for the linear power spectrum, since non-linearities become weaker.

In Fig. 6 we compare the linear (solid) and halofit (dashed) C_ℓ spectra for different redshifts at fixed spectroscopic bin width $\sigma_z = 10^{-3}$, going out to a well converged value of $k_{\text{max}} = 5$. As expected, the difference grows towards smaller redshift and higher multipoles. However, a constant offset remains even at low ℓ . This is better visible in Fig. 7, where we show the relative difference in %. At $z = 1$, spectroscopic power spectra show about 11.5% difference between the linear perturbation theory and the halofit power spectrum, even down to $\ell = 2$. At $\ell \gtrsim 100$, where non-linearities are expected to set in, this difference rapidly grows. Even at redshift $z = 5$ the difference between the linear and halofit power spectra still amounts to about 3% at $2 \leq \ell \leq 100$ and grows at higher ℓ 's.

4 Cross-correlations, $C_\ell(z_1, z_2)$ for $z_1 \neq z_2$

In this section we consider cross-correlations $C_\ell(z_1, z_2)$, with $z_1 \neq z_2$. It is well known that for widely separated redshifts, cross-correlations are dominated by the lensing–density (at low

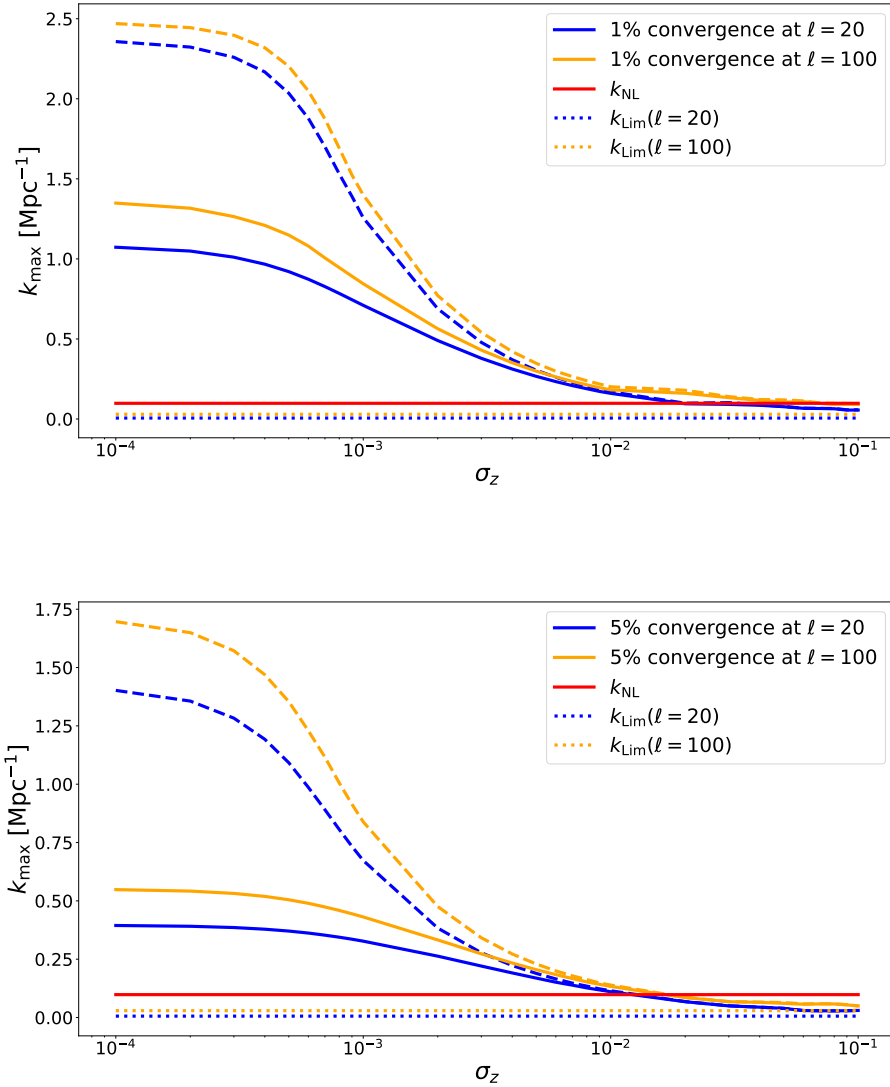


Figure 4. We show the values of k_{\max} required for $C_\ell(\bar{z} = 1, 10^{-4} < \sigma_z < 10^{-1})$ to converge to within 1% (upper panel) or 5% (lower panel) error, relative to the well-converged spectrum calculated with very high k_{\max} . We consider the values of the C_{20} (blue) and C_{100} (orange). The solid lines represent the linear spectra, while the dashed lines represent the halofit corrected spectra. We also plot with a red solid line the value of $k_{\text{NL}}(z)$ for $z = 1$. The dotted lines indicate the Limber value, $k_{\text{Lim}}(\ell, z)$, with the different colours corresponding to the two respective values of ℓ concerned.

redshifts) or the lensing–lensing (at high redshift) terms [14]. Furthermore, these terms are well approximated with the Limber approximation, to which only the spectrum at $k_{\text{Lim}} = (\ell + 1/2)/r(z)$ contributes [9]. Here we study just the standard terms, since only these may be affected by small scale contributions. The relation between the standard terms and the lensing terms depends on both galaxy bias $b(z)$ and magnification bias $s(z)$, which are survey dependent, see e.g. [4].

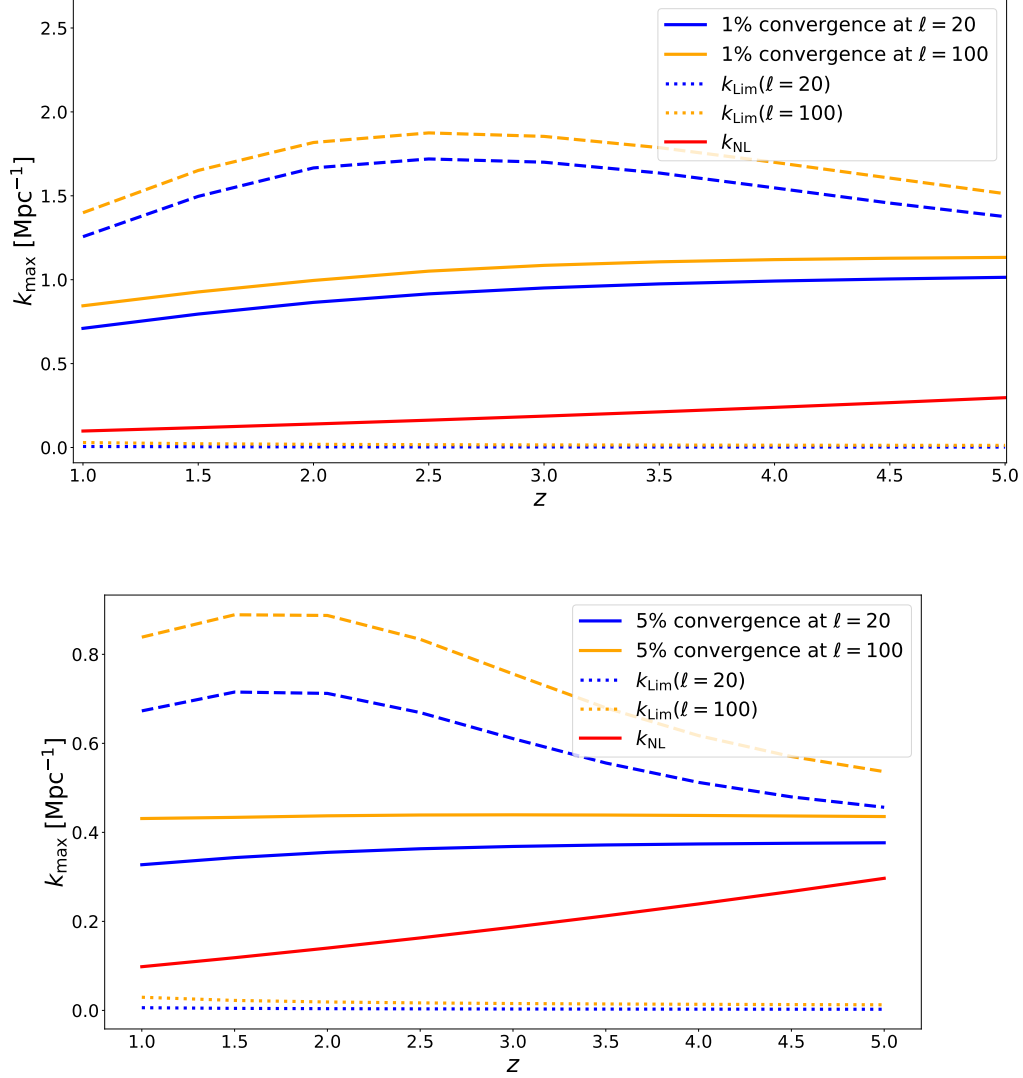


Figure 5. We show the values of k_{\max} required for $C_\ell(1.0 < \bar{z} < 5, \sigma_z = 10^{-3})$ to converge to within 1% (upper panel) or 5% (lower panel) error, relative to the spectrum calculated at high k , for C_{20} (blue) and C_{100} (orange). The solid lines represent the linear spectra, while the dashed lines represent the halo fit corrections. We plot with a red solid line the value of $k_{\text{NL}}(z)$ for the redshift range. The dotted lines indicate the Limber values $k_{\text{Lim}}(z, \ell)$ for the respective values of ℓ .

Therefore, we do not discuss their relative amplitude in this general study. We consider only redshift pairs (z_1, z_2) which are not too widely separated, so as to avoid cases where the contribution of the standard terms is completely negligible. In the Limber approximation, which is well known to fail for the standard terms in narrow redshift bins [9, 15], these terms simply vanish if the bins are not overlapping.

To obtain some intuition, we consider again the flat sky approximation and integrate over tophat windows of width σ_z centered at z_1 and z_2 . Setting $\bar{z} = (z_1 + z_2)/2$, a short calculation

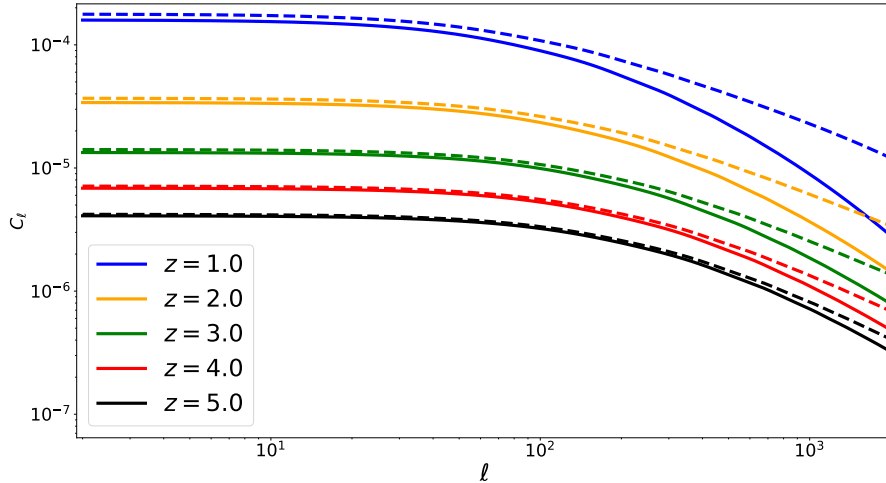


Figure 6. We show $C_\ell(\bar{z}, \sigma_z = 10^{-3})$ for various redshifts in the range $[1, 5]$. In solid lines we plot the linear power spectra, and in dashed lines the halofit spectra.

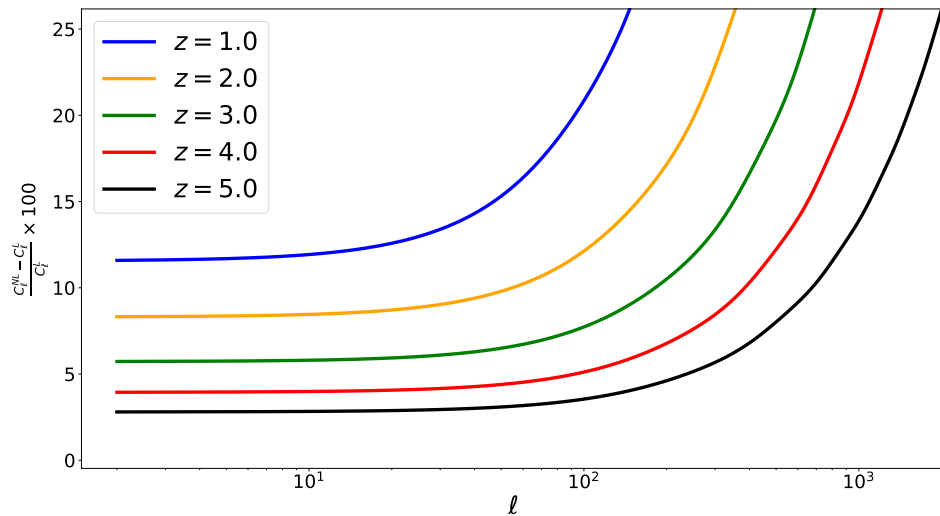


Figure 7. We show the relative differences between the linear (C_ℓ^L) and halofit (C_ℓ^{NL}) spectra in percent. Most importantly we see that the difference at low ℓ is about 11.5% at $z = 1$ and 8% at $z = 2$. Only at $z = 4$ does it drop below 5%.

gives

$$C_\ell(z_1, z_2, \sigma_z) \simeq \frac{1}{2\pi r^2(\bar{z})} \int_{-\infty}^{\infty} dk_{\parallel} P(k, \bar{z}) \exp\left(ik_{\parallel} \left(\frac{z_1}{H(z_1)} - \frac{z_2}{H(z_2)}\right)\right) j_0^2\left(\frac{k_{\parallel} \sigma_z}{2H(\bar{z})}\right). \quad (4.1)$$

In this approximation we have used that $H(z)$ and $P(k, z)$ change slowly with redshift, while the exponential changes rapidly. This approximation is not very accurate if z_1 and z_2 are not very close and we shall not use it for our numerical results. In addition to the low-pass filter $k_{\parallel}(z, \sigma_z) = 2\pi H(\bar{z})/\sigma_z$, we now have a new scale given by the wave number $k_{\times}(z_1, z_2)$, after which the exponential has performed about one oscillation,

$$k_{\times}(z_1, z_2) = \frac{2\pi H(\bar{z})}{|z_2 - z_1|} < \frac{2\pi H(\bar{z})}{\sigma_z} = k_{\parallel}(z, \sigma_z). \quad (4.2)$$

We assume that the two redshift bins are not overlapping, i.e. $|z_2 - z_1| > \sigma_z$. As a first guess one might hope that contributions from values of $k_{\parallel} > k_{\times}$ are averaged out by oscillations and can be neglected. The situation is actually quite interesting. To analyze it, let us first assume $P(k, z)$ to be independent of k_{\parallel} , a reasonable approximation for large ℓ , where $k \simeq \ell/r(z)$. In this case we can integrate (4.1) exactly. Defining

$$F(a) = \int_{-\infty}^{\infty} dx e^{ix} j_0^2(ax) = \begin{cases} 0 & a \leq 1/2 \\ \frac{\pi}{2a^2}(2a - 1) & a \geq 1/2, \end{cases} \quad (4.3)$$

we obtain

$$C_{\ell}(z_1, z_2, \sigma_z) \simeq \frac{H(\bar{z})}{2\pi|z_1 - z_2|r^2(\bar{z})} P(\ell/r(\bar{z}), \bar{z}) F\left(\frac{\sigma_z/2}{|z_1 - z_2|}\right), \quad (4.4)$$

which vanishes entirely for well separated windows, $\sigma_z < |z_1 - z_2|$. This corresponds to our findings for large $\ell > 100$, see Fig. 8, where a window size $\sigma_z = 10^{-3}$ is chosen. For smaller ℓ the situation is more complicated and the result depends entirely on the behavior of $P(k, z)$. Our numerical examples show that, depending on the redshift pair considered, the value k_{\max} required to achieve an accuracy of 10% for the cross-spectrum of the standard terms can be much smaller than k_{\times} or up to more than 8 times higher.

The contribution from the standard terms in the cross-correlations are very small and tend to zero for $\ell \gtrsim 100$, see Fig. 8. Thus, measuring these terms with observations will be quite challenging. For this reason, we only investigate the k_{\max} needed for a 10% accuracy in this case. Also, as the signal is very close to zero at $\ell = 100$, we concentrate on the case $\ell = 20$ which is also more relevant here, as it is typically expected to converge for smaller values of k_{\max} .

The k_{\max} needed to achieve 10% accuracy in the spectrum is about $8k_{\times}$ for $(z_1, z_2) = (2, 2.3)$ and $\ell = 20$; however, it remains smaller than k_{NL} , so we deduce that non-linearities are not important at low ℓ , see Fig. 9. For $(z_1, z_2) = (1, 1.1)$, k_{\max} is much smaller than k_{\times} , actually roughly given by k_{Lim} , which would be in agreement with our naive expectation. It seems then that the scale k_{\times} does not characterise the scale of important contributions well, if at all. While the reason for this is not entirely clear to the authors, one point is simply that the cross-correlation signal of density and redshift space distortion for $(z_1, z_2) = (2, 2.3)$ is about 10 times smaller than the one for $(z_1, z_2) = (1, 1.1)$ for $\ell = 20$, making an accuracy of 10% even more difficult to attain. We also found that, when considering higher redshifts, e.g. $\bar{z} \sim 3$, it is possible for k_{\max} to decrease again to less than k_{\times} and, when considering a smaller separation $(z_1, z_2) = (2, 2.2)$, where the standard terms are larger, we find a very small k_{\max} , once more in agreement with our naive expectation.

However, the accuracy of the standard terms is not so relevant for cross-correlation spectra, something which should be borne in mind when interpreting the values of k_{\max} in this section. First of all, as already mentioned, the lensing signal cannot be neglected in these spectra and

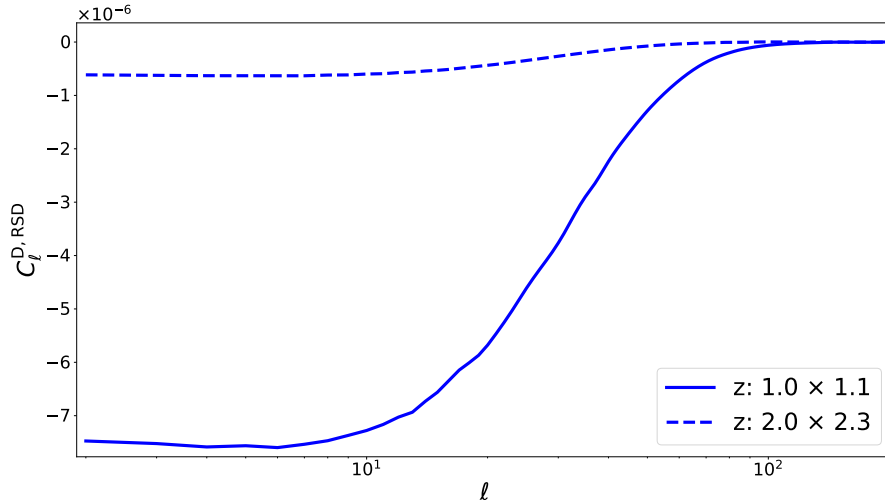


Figure 8. We show the angular power spectrum for the redshift pairs: $(z_1 = 1, z_2 = 1.1)$ and $(z_1 = 2, z_2 = 2.3)$. Only density and redshift space distortions are included in the signal here, and a window of $\sigma_z = 10^{-3}$ is chosen. At $\ell \gtrsim 100$ the contribution from these terms is much less significant.

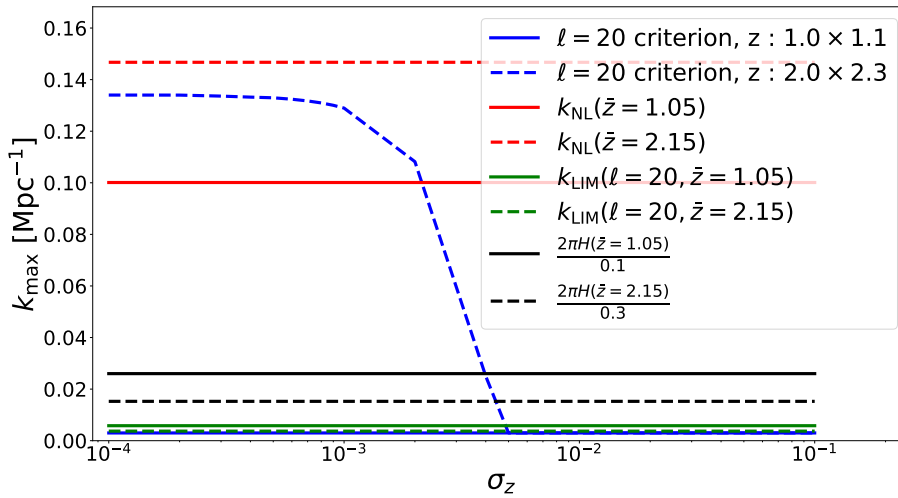


Figure 9. We show the value of k_{\max} needed to achieve a 10% precision for the cross-correlation spectrum $C_{20}(z_1, z_2)$ at $(z_1 = 1, z_2 = 1.1)$ and $(z_1 = 2, z_2 = 2.3)$ as a function of the window width σ_z . Here only density and redshift space distortions are included in the signal.

including it significantly enhances the total signal, increasing the accuracy in calculating the total signal of the Limber approximation, which requires a lower k_{\max} . In Fig. 10 we show as an example the proportional contribution of the standard terms, $C_\ell^{\text{D,RSD}}$, to the total spectrum including also the lensing terms, with values for $b(z)$ and $s(z)$ for SKAII as given in [16], Appendix A4. We use

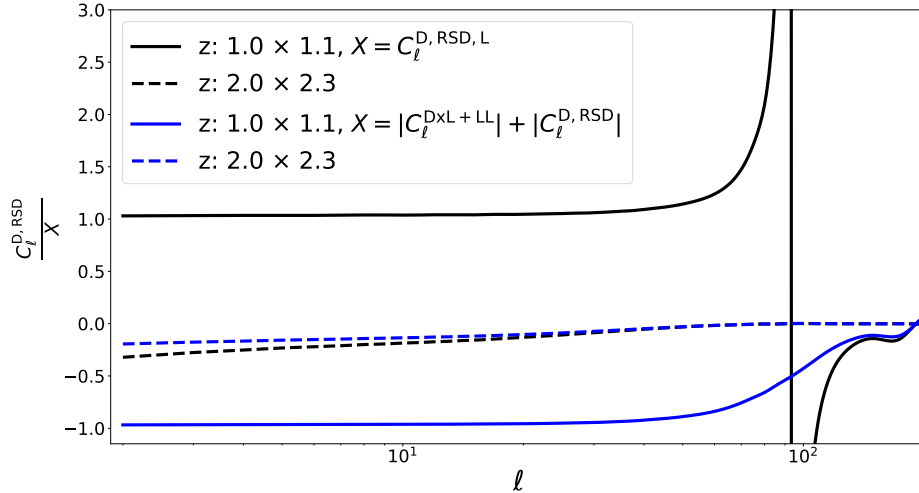


Figure 10. We show the fraction of the full angular power spectrum made up for by the density and redshift space distortion terms, in the case of an SKAII-like spectroscopic galaxy survey (black). Since the total signal vanishes at $\ell \sim 100$, we also show $C_\ell^{D,RSD} / (|C_\ell^{D,RSD}| + |C_\ell^{L \times D + LL}|)$ (blue).

the same redshift pairs as for the previous figures (black lines). For $(z_1, z_2) = (1, 1.1)$, at low ℓ , the ratio is slightly larger than 1, since the lensing contribution, dominated by the density-lensing cross-correlation, is negative. The divergence at $\ell \simeq 100$ is the consequence of a zero-crossing of the denominator, the total spectrum. To remove it we also plot $C_\ell^{D,RSD} / (|C_\ell^{D,RSD}| + |C_\ell^{L \times D + LL}|)$ (blue lines). At $\ell > 120$, the total signal is positive, the lensing term now dominates and the standard terms contribute less than about 20%. For $(z_1, z_2) = (2, 2.3)$ the lensing term is always positive and dominates. The standard terms contribute only about 13% already for $\ell \gtrsim 20$, so that a 10% error in the standard terms leads to a 1.3% error in the total result. Assuming a numerical accuracy of about 1% for these cross-correlations, it is not clear whether the high value of k_{\max} found in this case should not be (at least partially) attributed to numerical error in the CAMB-code with which the spectra have been computed. For $(z_1, z_2) = (2, 2.2)$ the standard terms still contribute nearly 50% at $\ell = 20$ and the required k_{\max} is again very small, while for $(z_1, z_2) = (2, 2.5)$ they are below 5%, while the required k_{\max} is even larger than that for $(z_1, z_2) = (2, 2.3)$. But as mentioned above, these percentages depend on $b(z)$ and $s(z)$.

The second reason why the accuracy of the standard terms is not of utmost importance, is that cross-correlations cannot be measured as accurately as auto-correlations, due to cosmic variance. The cosmic variance of cross-correlations is dominated by the much larger auto-correlations,

$$\text{Var}(C_\ell(z_1, z_2)) \simeq \frac{C_\ell(z_1, z_1)C_\ell(z_2, z_2)}{2\ell + 1}. \quad (4.5)$$

For example at $z \simeq 1$, $\Delta z \geq 0.1$ and $\ell \leq 50$ auto-correlations are of the order of 10^{-4} while cross-correlations are about 10^{-7} . Hence, for a given redshift combination and $\ell \sim 20$, we expect a signal-to-noise ratio from the standard term alone of less than 0.1. To overcome this large cosmic variance, one would have to consider significant binning in ℓ - and z -space.

5 Conclusion

In this paper we have studied the angular power spectra for galaxy number counts, $C_\ell(z, z')$. In particular, we have investigated their dependence on the widths of the considered redshift window, σ_z . We have found that in slim windows, relevant for spectroscopic surveys, i.e. $\sigma_z \simeq 10^{-3}$, the spectra are strongly affected by non-linearities coming from high values of k , i.e. small scales, even down to $\ell = 2$. This is especially true in the case of equal redshifts, $z = z'$, and much less so for cross-correlations of different redshifts that are non-overlapping, but still close enough so that the standard density+RSD terms in the number counts are nevertheless considerable. Such spectroscopic surveys are very important to measure the growth rate of perturbations, one of the most interesting variables to distinguish between different dark energy models [16–18].

Our finding is an additional motivation to use, instead of the angular power spectrum, the correlation function, which is not affected by non-linearities for sufficiently large separations, in the analysis of spectroscopic surveys. This has been advocated already in the past [19, 20]. In Ref. [20] a public code for the fully-relativistic correlation function is presented and a significant speedup of this code has been recently achieved [21]. Another argument for why the angular power spectra are not suited for spectroscopic redshift resolution is the fact that even in very big surveys we would at best have a few thousand galaxies per redshift bin with $\sigma_z \simeq 10^{-3}$ which leads to very substantial shot noise.

For cross-correlations, the value of k_{\max} needed to achieve a precision of 10% for the density and RSD contribution to the $C_\ell(z, z')$ is not so high due to the following reasons: 1) The cross-correlation signal has an additional oscillating function in its integral, which reduces the contributions from high k_{\parallel} . 2) The lensing terms of cross-correlations, that are well approximated by the Limber approximation, are much more significant than their contribution to auto-correlations and so the k_{\max} needed for a 10% precision of the total, measured power spectra is significantly smaller. 3) Finally, the cross-correlation signal is much smaller than the auto-correlation signal, while its cosmic variance is similar. Therefore, we expect to achieve significantly lower precision in the measurements of cross-correlations. For these reasons, we have determined the value k_{\max} required to achieve 10% precision for the contribution of the standard terms to cross-correlations. At large redshift differences, cross-correlations are dominated by the lensing term and one can safely apply the Limber approximation to compute them, see [9] for a detailed study.

We therefore consider our results very important for the auto-correlations which will be measured with a high signal-to-noise ratio in upcoming spectroscopic surveys like Euclid or SKA, but not so relevant for cross-correlations of non-overlapping redshift bins.

Acknowledgements

It is a pleasure to thank Martin Kunz and Francesca Lepori for enlightening discussions. The authors acknowledge financial support from the Swiss National Science Foundation grant no. 200020-182044

References

- [1] C. Bonvin and R. Durrer, *What galaxy surveys really measure*, *Phys. Rev.* **D84** (2011) 063505, [[arXiv:1105.5280](#)].
- [2] A. Challinor and A. Lewis, *The linear power spectrum of observed source number counts*, *Phys. Rev.* **D84** (2011) 043516, [[arXiv:1105.5292](#)].

- [3] D. Jeong, F. Schmidt, and C. M. Hirata, *Large-scale clustering of galaxies in general relativity*, *Phys. Rev.* **D85** (2012) 023504, [[arXiv:1107.5427](#)].
- [4] E. Di Dio, F. Montanari, J. Lesgourgues, and R. Durrer, *The CLASSgal code for Relativistic Cosmological Large Scale Structure*, *JCAP* **1311** (2013) 044, [[arXiv:1307.1459](#)].
- [5] E. Di Dio, F. Montanari, R. Durrer, and J. Lesgourgues, *Cosmological Parameter Estimation with Large Scale Structure Observations*, *JCAP* **1401** (2014) 042, [[arXiv:1308.6186](#)].
- [6] D. Alonso, P. Bull, P. G. Ferreira, R. Maartens, and M. Santos, *Ultra large-scale cosmology in next-generation experiments with single tracers*, *Astrophys. J.* **814** (2015), no. 2 145, [[arXiv:1505.07596](#)].
- [7] C. S. Lorenz, D. Alonso, and P. G. Ferreira, *The impact of relativistic effects on cosmological parameter estimation*, [arXiv:1710.02477](#).
- [8] M. Jalilvand, B. Ghosh, E. Majerotto, B. Bose, R. Durrer, and M. Kunz, *Nonlinear contributions to angular power spectra*, *Phys. Rev. D* **101** (2020), no. 4 043530, [[arXiv:1907.13109](#)].
- [9] W. L. Matthewson and R. Durrer, *The Flat Sky Approximation to Galaxy Number Counts*, *JCAP* **02** (2021) 027, [[arXiv:2006.13525](#)].
- [10] R. Durrer, *The Cosmic Microwave Background*. Cambridge University Press, 12, 2020.
- [11] D. Blas, J. Lesgourgues, and T. Tram, *The Cosmic Linear Anisotropy Solving System (CLASS) II: Approximation schemes*, *JCAP* **1107** (2011) 034, [[arXiv:1104.2933](#)].
- [12] **Euclid** Collaboration, R. Laureijs et al., *Euclid Definition Study Report*, [arXiv:1110.3193](#).
- [13] A. Rassat, A. Amara, L. Amendola, F. J. Castander, T. Kitching, M. Kunz, A. Refregier, Y. Wang, and J. Weller, *Deconstructing Baryon Acoustic Oscillations: A Comparison of Methods*, [arXiv:0810.0003](#).
- [14] F. Montanari and R. Durrer, *Measuring the lensing potential with tomographic galaxy number counts*, *JCAP* **1510** (2015), no. 10 070, [[arXiv:1506.01369](#)].
- [15] E. Di Dio, R. Durrer, R. Maartens, F. Montanari, and O. Umeh, *The Full-Sky Angular Bispectrum in Redshift Space*, *JCAP* **1904** (2019) 053, [[arXiv:1812.09297](#)].
- [16] G. Jelic-Cizmek, F. Lepori, C. Bonvin, and R. Durrer, *On the importance of lensing for galaxy clustering in photometric and spectroscopic surveys*, [arXiv:2004.12981](#).
- [17] A. Cooray, D. Huterer, and D. Baumann, *Growth rate of large scale structure as a powerful probe of dark energy*, *Phys. Rev. D* **69** (2004) 027301, [[astro-ph/0304268](#)].
- [18] C. Di Porto and L. Amendola, *Observational constraints on the linear fluctuation growth rate*, *Phys. Rev. D* **77** (2008) 083508, [[arXiv:0707.2686](#)].
- [19] V. Tansella, C. Bonvin, R. Durrer, B. Ghosh, and E. Sellentin, *The full-sky relativistic correlation function and power spectrum of galaxy number counts. Part I: theoretical aspects*, *JCAP* **1803** (2018), no. 03 019, [[arXiv:1708.00492](#)].
- [20] V. Tansella, G. Jelic-Cizmek, C. Bonvin, and R. Durrer, *COFFE: a code for the full-sky relativistic galaxy correlation function*, *JCAP* **1810** (2018), no. 10 032, [[arXiv:1806.11090](#)].
- [21] G. Jelic-Cizmek, *The flat-sky approximation to galaxy number counts - redshift space correlation function*, [arXiv:2011.01878](#).